Solving the Bethe-Salpeter equation for the second-harmonic generation in Zn chalcogenides

A. Riefer* and W. G. Schmidt
Department Physik, Universität Paderborn, 33095 Paderborn, Germany
(Received 20 September 2017; revised manuscript received 23 November 2017; published 19 December 2017)

The influence of excitonic and local-field effects on the second-harmonic-generation spectrum of zinc-blende ZnS, ZnSe, and ZnTe is studied from first principles using the Bethe-Salpeter equation. The calculations are based on the theory of R. Leitsmann *et al.* [Phys. Rev. B **71**, 195209 (2005)], which we extended to the low-frequency range. The dielectric function and the second-harmonic-generation spectrum have been obtained within the independent (quasi)particle approximation and within the Bethe-Salpeter approach. The calculations demonstrate that the linear and the nonlinear optical properties are similarly affected by excitonic and local-field effects. The computed spectra are furthermore compared with measurements and calculations within the time-dependent density-polarization functional theory (TD-DPFT) in the real-time framework. The present approach most commonly suggests stronger excitonic effects than observed in the real-time TD-DPFT calculations, while local-field corrections are comparably described. Although agreement is found between the Bethe-Salpeter spectra and measurements for the dielectric function, deviations from the experimental data are observed for second-harmonic generation.

DOI: 10.1103/PhysRevB.96.235206

I. INTRODUCTION

For several years one has been able to calculate the linear optical response from first principles by considering excitonic and crystal local-field effects along with the full quasiparticle band structure [1–4]. Within the many-body perturbation theory (MBPT), the quasiparticle (QP) levels are obtained by solving the QP equation [5,6], typically in the GW approximation [7]. Based on the quasiparticle levels, excitonic and local-field effects can be accounted for by solving the Bethe-Salpeter equation (BSE) [8–10]. This approach is highly successful for the linear optical properties of various bulk materials, surfaces, and molecules [1–4,11].

On the other hand, the technique of second-order nonlinear optical spectroscopy, e.g., the second-harmonic generation (SHG), is a powerful tool in the experimental characterization of materials due to its sensitivity for surfaces and interfaces [12,13]. Presently, only a few SHG calculations go beyond the independent (quasi)particle level of theory: Luppi *et al.* [14] suggested an approach to calculate SHG within response theory and the time-dependent density functional theory (TDDFT), which was applied to compute the SHG spectra of the cubic bulk materials SiC, GaAs, and AlAs, observing the essential influence of excitonic and local-field effects.

Attaccalite and Grüning [15] and Attaccalite *et al.* [16] formulated a real-time framework where the response functions are obtained from the dynamical polarization by numerical integration of the equations of motion for the Kohn-Sham states. In that way, higher-order response functions are calculated without additional computational effort, and excitonic as well as local-field effects in the SHG spectrum are accounted for using an appropriate effective Hamiltonian [17–19]. Recently, the SHG spectra of zinc-blende ZnS, ZnSe, and ZnTe have been calculated within the time-dependent density-polarization functional theory (TD-DPFT) in the real-time framework [20].

SHG calculations based on MBPT have been performed by Leitsmann *et al.* [21] and Chang *et al.* [22], who used the Bethe-Salpeter approach, to compute the SHG spectrum of bulk GaAs and additionally of AlP, AlAs, and GaP. Furthermore, Trolle *et al.* [23] studied the nonlinear optical properties of monolayer MoS_2 with a theory similar to that in Ref. [21].

The aim of the present study is to investigate the impact of excitonic and local-field effects on the SHG spectra from MBPT with the BSE approach. We use the zinc-blende Zn chalcogenides as model systems since there are both measured spectra [24] and results within the real-time TD-DPFT framework [20] available for comparison. Furthermore, a simplified three-band Wannier exciton model for ZnS (and other cubic semiconductors) suggests the importance of excitonic effects in the SHG spectrum [25]. Methodologically, we use the formalism of Leitsmann *et al.* [21], which is based on MBPT and response theory [26]. To obtain the SHG spectra within this approach, it is necessary to evaluate *three-particle Green's-function*-like expectation values, which are approximated with the aid of interacting electron-hole pair states from the solution of the Bethe-Salpeter equation. An issue of the present paper is the extension of this formalism to low frequencies: We remove the divergence for the limit $\omega \to 0$ present in the derivation in Ref. [21]. Ground-state properties and quasiparticle band energies, on which the determination of the optical response is based, are obtained with hybrid DFT [27–29] (HSE03) and by a perturbative solution of the QP equation (G_0W_0 method [30–32]).

This paper is structured as follows: We present the analytic derivation and provide implementation details for the present approach in Sec. II. The parameters for the ground-state and quasiparticle calculations as well as for the computation of the optical response are summarized in Sec. III. The results are discussed in Sec. IV, and the conclusions are given in Sec. V.

II. THEORY

A. SHG equations including excitonic and local-field effects

The second-harmonic-generation process can be described by the quadratic susceptibility tensor [26] $\chi^{(2)}(-\omega;\omega_1,\omega_2)$.

*riefer@mail.upb.de

The components $P_\alpha^{(2)}(t)$ of the second-order polarization are given for an incident monochromatic field $\mathbf{E}(t) = \mathbf{E}_0\, e^{-i\omega t}$ and crystals with the zinc-blende structure by

$$P_x^{(2)}(t) = \sum_{\beta\gamma} \chi^{(2)}_{x\beta\gamma}(-2\omega;\omega,\omega) E_\beta(t) E_\gamma(t) \tag{1}$$

$$= 2\chi^{(2)}_{xyz}(-2\omega;\omega,\omega) E_y(t) E_z(t), \tag{2}$$

with analogous notation for P_y and P_z. $\chi^{(2)}_{\alpha\beta\gamma}(-2\omega;\omega,\omega)$ is the second-harmonic-generation tensor. The intrinsic permutation symmetry, i.e., $\chi^{(2)}_{xyz} = \chi^{(2)}_{xzy}$, has been applied from (1) to (2).

The Hamiltonian describing the interaction of optically excited electrons and holes within the BSE approach is given by [1–4]

$$H^{\mathrm{ex}}_{vc\mathbf{k},v'c'\mathbf{k}'} = (\epsilon_{c\mathbf{k}} - \epsilon_{v\mathbf{k}})\delta_{vv'}\delta_{cc'}\delta_{\mathbf{k},\mathbf{k}'} + 2\iint d\mathbf{r}d\mathbf{r}'\psi^*_{c\mathbf{k}}(\mathbf{r})\psi_{v\mathbf{k}}(\mathbf{r})\bar{v}(\mathbf{r}-\mathbf{r}')\psi_{c'\mathbf{k}'}(\mathbf{r}')\psi^*_{v'\mathbf{k}'}(\mathbf{r}')$$
$$- \iint d\mathbf{r}d\mathbf{r}'\psi^*_{c\mathbf{k}}(\mathbf{r})\psi_{c'\mathbf{k}'}(\mathbf{r})W(\mathbf{r},\mathbf{r}')\psi_{v\mathbf{k}}(\mathbf{r}')\psi^*_{v'\mathbf{k}'}(\mathbf{r}'). \tag{3}$$

The first term describes the excitation of noninteracting (quasi)particles with the respective energies $\epsilon_{v\mathbf{k}}$ and $\epsilon_{c\mathbf{k}}$ at a point $\mathbf{k}$ of the Brillouin zone (BZ). The second and the third terms with the statically screened Coulomb potential $W(\mathbf{r},\mathbf{r}')$ and the nonsingular part of the bare Coulomb potential $\bar{v}(\mathbf{r}-\mathbf{r}')$ account for the electron-hole attraction and the crystal local-field effects, respectively. The matrix elements are evaluated from the wave functions $\psi_{v\mathbf{k}}$ and $\psi_{c\mathbf{k}}$ of valence and conduction states.

Now, one can define the two auxiliary functions,

$$\Pi_\alpha(\Lambda,cv\mathbf{k}) := A^{cv}_\Lambda(\mathbf{k}) \sum_{c'v'\mathbf{k}'} p^\alpha_{c'v'}(\mathbf{k}') \left[A^{c'v'}_\Lambda(\mathbf{k}')\right]^* \tag{4}$$

and

$$Z_{\alpha\beta\gamma}(\Lambda,\Lambda',cv\mathbf{k}) := [\Pi_\alpha(\Lambda,cv\mathbf{k})]^* \left[\sum_{c'} \Pi_\beta(\Lambda',c'v\mathbf{k}) p^\gamma_{cc'}(\mathbf{k}) - \sum_{v'} \Pi_\beta(\Lambda',cv'\mathbf{k}) p^\gamma_{v'v}(\mathbf{k})\right], \tag{5}$$

where $A^{cv}_\Lambda(\mathbf{k})$ are the eigenfunctions to the eigenvalues E_Λ of the exciton Hamiltonian and $p^\alpha_{nm}(\mathbf{k})$ are the momentum matrix elements. Additionally, we define

$$Z_{\alpha\beta\gamma}(\Lambda,\Lambda') := \sum_{cv\mathbf{k}} Z_{\alpha\beta\gamma}(\Lambda,\Lambda',cv\mathbf{k}). \tag{6}$$

The auxiliary functions allow the following representation of the second-harmonic-generation tensor within the BSE approach [as given by Eq. (42) of Ref. [21]]:

$$\chi^{(2)}_{\alpha\beta\gamma}(-2\omega;\omega,\omega) = -\frac{ie^3\hbar^3}{2m_e^3 V} \sum_{\Lambda,\Lambda'} \sum_{cvk} \{A(\hbar\tilde{\omega},E_\Lambda,E_{\Lambda'})[Z_{\alpha\beta\gamma}(\Lambda',\Lambda) + Z_{\alpha\gamma\beta}(\Lambda',\Lambda)]^*$$
$$- A(-\hbar\tilde{\omega},E_\Lambda,E_{\Lambda'})[Z_{\alpha\beta\gamma}(\Lambda',\Lambda) + Z_{\alpha\gamma\beta}(\Lambda',\Lambda)]$$
$$- B(\hbar\tilde{\omega},E_\Lambda,E_{\Lambda'})[Z_{\beta\gamma\alpha}(\Lambda',\Lambda) + Z_{\gamma\beta\alpha}(\Lambda',\Lambda)]^* + B(-\hbar\tilde{\omega},E_\Lambda,E_{\Lambda'})[Z_{\beta\gamma\alpha}(\Lambda',\Lambda) + Z_{\gamma\beta\alpha}(\Lambda',\Lambda)]\}. \tag{7}$$

The functions A and B are given by

$$A(\hbar\tilde{\omega},E_\Lambda,E_{\Lambda'}) = \frac{1}{(E_\Lambda + \hbar\tilde{\omega})(E_{\Lambda'} + 2\hbar\tilde{\omega})(\hbar\tilde{\omega})^3}, \tag{8}$$

$$B(\hbar\tilde{\omega},E_\Lambda,E_{\Lambda'}) = \frac{1}{(E_\Lambda - E_{\Lambda'} + 2\hbar\tilde{\omega})(E_\Lambda + \hbar\tilde{\omega})(\hbar\tilde{\omega})^3}, \tag{9}$$

and the frequency ω is shifted by the positive broadening η, i.e., $\tilde{\omega} = \omega + i\eta$. Equation (7) also exploits that

$$Z_{\alpha\beta\gamma}(\Lambda,\Lambda') = [Z_{\beta\alpha\gamma}(\Lambda',\Lambda)]^*, \tag{10}$$

utilizing $p^\alpha_{nm}(\mathbf{k}) = [p^\alpha_{mn}(\mathbf{k})]^*$.

The SHG tensor (7) becomes divergent for frequencies $\omega \to 0$ due to the factor $\tilde{\omega}^{-3}$ in the functions A and B. In order to lift this divergence, we perform a partial fraction expansion for functions A and B following the procedure proposed by Ghahramani *et al.* [33] and Aspnes [34] for the independent particle approximation (IPA). A and B can be expressed as

$$A(\hbar\tilde{\omega},E_\Lambda,E_{\Lambda'}) = \sum_{i=1,\ldots,5} A_i(\hbar\tilde{\omega},E_\Lambda,E_{\Lambda'}), \tag{11}$$

$$B(\hbar\tilde{\omega},E_\Lambda,E_{\Lambda'}) = \sum_{i=1,\ldots,5} B_i(\hbar\tilde{\omega},E_\Lambda,E_{\Lambda'}). \tag{12}$$

The functions A_i and B_i are given in Appendix A. Appendix A also shows that A_1, A_2, and B_1 are the only nonvanishing contributions to the SHG tensor for crystals exhibiting the zinc-blende structure. The cancellation of the divergent contributions related to A_4 and B_4 requires this special crystal symmetry. We mention that Ghahramani *et al.* [33] proved the vanishing of related divergent terms for the IPA approach using $\mathbf{k}\cdot\mathbf{p}$ perturbation theory and finding an appropriate potential [see Eq. (A5) of Ref. [33]]. Analogous access for the BSE approach has not been found within this study.

Employing the results above, the SHG tensor is given by

$$\begin{aligned}\chi^{(2)}_{\alpha\beta\gamma}(-2\omega;\omega,\omega) = -\frac{ie^3\hbar^3}{2m_e^3V}\sum_{\Lambda,\Lambda'}\Bigg\{&\frac{1}{(2E_{\Lambda'}-E_\Lambda)}\left[\frac{1}{E^3_{\Lambda'}(E_{\Lambda'}+\hbar\tilde\omega)}-\frac{16}{E^3_\Lambda(E_\Lambda+2\hbar\tilde\omega)}\right][Z_{\alpha\beta\gamma}(\Lambda,\Lambda')^*+Z_{\alpha\gamma\beta}(\Lambda,\Lambda')^*]\\ &-\frac{1}{(2E_{\Lambda'}-E_\Lambda)}\left[\frac{1}{E^3_{\Lambda'}(E_{\Lambda'}-\hbar\tilde\omega)}-\frac{16}{E^3_\Lambda(E_\Lambda-2\hbar\tilde\omega)}\right][Z_{\alpha\beta\gamma}(\Lambda,\Lambda')+Z_{\alpha\gamma\beta}(\Lambda,\Lambda')]\\ &-\frac{1}{(E_\Lambda+E_{\Lambda'})}\left[\frac{1}{E^3_\Lambda(E_\Lambda+\hbar\tilde\omega)}-\frac{1}{E^3_{\Lambda'}(E_{\Lambda'}-\hbar\tilde\omega)}\right][Z_{\beta\gamma\alpha}(\Lambda,\Lambda')+Z_{\beta\gamma\alpha}(\Lambda',\Lambda)^*]\Bigg\}. \end{aligned} \tag{13}$$

It is straightforward to obtain the expression for $\chi^{(2)}$ within the IPA from Eq. (13): Since the exciton Hamiltonian H^{ex} is diagonal in the case of IPA, one can apply the replacement

$$\text{IPA:}\quad A^{cv}_\Lambda(\mathbf{k}) = \delta_{cv\mathbf{k},\Lambda},\quad E_{cv\mathbf{k}} = \epsilon_{c\mathbf{k}} - \epsilon_{v\mathbf{k}}, \tag{14}$$

so that it follows for the auxiliary function Π

$$\text{IPA:}\quad \Pi_\alpha(\Lambda, cv\mathbf{k}) = p^\alpha_{cv}(\mathbf{k})\,\delta_{cv\mathbf{k},\Lambda}. \tag{15}$$

Continuing in this way, one obtains the IPA-SHG equations in the formalism of Leitsmann *et al.* The details are given in Appendix B. The equivalence to the IPA equations of Ghahramani *et al.* [33] and Aspnes [34] is also shown in Ref. [21].

Furthermore, applying time-reversal symmetry, Eq. (13) can be further simplified to the expression

$$\begin{aligned}\chi^{(2)}_{\alpha\beta\gamma}(-2\omega;\omega,\omega) = -\frac{e^3\hbar^3}{2m_e^3V}\sum_{\Lambda,\Lambda'}\sum_{s=\pm1}\Bigg(&\frac{1}{E_\Lambda+E_{\Lambda'}}\left[\frac{1}{E^3_\Lambda(E_\Lambda+s\hbar\tilde\omega)}-\frac{1}{E^3_{\Lambda'}(E_{\Lambda'}-s\hbar\tilde\omega)}\right]\mathrm{Im}[Z_{\beta\gamma\alpha}(\Lambda,\Lambda')]\\ &+\frac{1}{2E_{\Lambda'}-E_\Lambda}\left[\frac{1}{E^3_{\Lambda'}(E_{\Lambda'}+s\hbar\tilde\omega)}-\frac{16}{E^3_\Lambda(E_\Lambda+2s\hbar\tilde\omega)}\right]\{\mathrm{Im}[Z_{\alpha\beta\gamma}(\Lambda,\Lambda')]+\mathrm{Im}[Z_{\alpha\gamma\beta}(\Lambda,\Lambda')]\}\Bigg), \end{aligned} \tag{16}$$

as shown in Appendix C.

B. Computation of the SHG spectrum

The exciton Hamiltonian (3) has to be diagonalized for the computation of the SHG spectrum. Having obtained the eigenvector-eigenvalue pairs, the SHG spectrum can be calculated from Eq. (13) or Eq. (16). The numerical effort of these computations is analyzed in the following. Defining the two matrices

$$\mathscr{E}_{k,a,b,n}(\hbar\tilde\omega;\Lambda,\Lambda') := \frac{k}{(a\,E_\Lambda + b\,E_{\Lambda'})E^3_\Lambda}\,\frac{1}{(E_\Lambda + n\,\hbar\tilde\omega)} \tag{17}$$

and

$$\begin{aligned}\Gamma_{\beta\gamma}(\Lambda', cv\mathbf{k}) :=& \sum_{c'}\Pi_\beta(\Lambda', c'v\mathbf{k})p^\gamma_{cc'}(\mathbf{k})\\ &-\sum_{v'}\Pi_\beta(\Lambda', cv'\mathbf{k})p^\gamma_{v'v}(\mathbf{k}), \end{aligned} \tag{18}$$

where k,a,b,n are real numbers, the subsequent expression characteristic for Eq. (13) can be written in matrix formalism,

$$\begin{aligned}&\sum_{\Lambda,\Lambda'}\frac{k}{(a\,E_\Lambda + b\,E_{\Lambda'})E^3_\Lambda}\,\frac{1}{(E_\Lambda + n\,\hbar\tilde\omega)}\sum_{cvk}Z_{\alpha\beta\gamma}(\Lambda,\Lambda',cv\mathbf{k})\\ &\quad=\mathrm{Tr}\big\{\mathscr{E}(\hbar\tilde\omega)\big[\Gamma_{\beta\gamma}\Pi^+_\alpha\big]\big\}. \end{aligned} \tag{19}$$

The dependency of $\mathscr{E}$ on the constants k,a,b,n is suppressed, and it is used for the trace of a matrix M in Eq. (19): $\mathrm{Tr}[M] = \sum_\Lambda M_{\Lambda,\Lambda}$. It is evident from Eq. (19) that setting aside the ω-dependent matrix $\mathscr{E}$, the leading order of computational effort is three matrix-matrix multiplications to obtain $Z_{\alpha\beta\gamma}$, $Z_{\alpha\gamma\beta}$, and $Z_{\beta\gamma\alpha}$. Focusing on computation time, we use BLAS routines and MPI parallelization for the evaluation of the algebraic operations. However, this requires additional memory for the storage of the matrices Π, Γ, and $Z = \Gamma\cdot\Pi^+$, which have the size of the excitonic matrix (3).

Since the differences $(2E_\Lambda - E_{\Lambda'})$ in the denominators of Eqs. (13) and (16) can cause divergent or singular numerical results for positive excitonic eigenvalues E_Λ, such cases for E_Λ and $E_{\Lambda'}$ have to be handled separately. Exploiting the limit

$$\begin{aligned}&\lim_{E_{\Lambda'}\to 2E_\Lambda}[A_1(\hbar\tilde\omega,E_\Lambda,E_{\Lambda'}) + A_2(\hbar\tilde\omega,E_\Lambda,E_{\Lambda'})]\\ &\quad=\frac{-1}{2}\,\frac{3\hbar\tilde\omega+4E_\Lambda}{E^4_\Lambda(E_\Lambda+\hbar\tilde\omega)^2} =: A^{\mathrm{corr}}(\hbar\tilde\omega,E_\Lambda), \end{aligned} \tag{20}$$

we use the correction term

$$\begin{aligned}&\chi^{(2),\mathrm{corr}}_{\alpha\beta\gamma}(-2\omega,\omega,\omega)\\ &\quad=-\frac{ie^3\hbar^3}{2m_e^3V}\sum_{|2E_{\Lambda'}-E_\Lambda|<\eta}\\ &\qquad\times\{A^{\mathrm{corr}}(\hbar\tilde\omega,E_{\Lambda'})[Z_{\alpha\beta\gamma}(\Lambda,\Lambda')^* + Z_{\alpha\gamma\beta}(\Lambda,\Lambda')^*]\\ &\qquad-A^{\mathrm{corr}}(-\hbar\tilde\omega,E_{\Lambda'})[Z_{\alpha\beta\gamma}(\Lambda,\Lambda') + Z_{\alpha\gamma\beta}(\Lambda,\Lambda')]\} \end{aligned} \tag{21}$$

$$= -\frac{e^3\hbar^3}{2m_e^3 V} \sum_{|2E_{\Lambda'}-E_\Lambda|<\eta} \sum_{s=\pm 1} \times A^{\mathrm{corr}}(s\hbar\tilde{\omega}, E_{\Lambda'})\{\mathrm{Im}[Z_{\alpha\beta\gamma}(\Lambda,\Lambda')]+\mathrm{Im}[Z_{\alpha\gamma\beta}(\Lambda,\Lambda')]\} \quad (22)$$

to account for contributions with $|2E_{\Lambda'} - E_\Lambda| < \eta$ in the numerical calculations. The expression (22) follows from (21) by utilizing time-reversal symmetry similar to that for Eq. (16). The correction contribution causes a small but visible change in the line shape on the IPA level but is essential within the BSE approach to ensure the stability of the numerical calculations.

III. COMPUTATION

Our purpose is to study the nonlinear optical properties of the three zinc-blende-type wide-band-gap semiconductors, ZnS, ZnSe, and ZnTe, with the methods presented in Sec. II. Recently, the SHG spectrum was measured [24] and calculated within the TDDFT [20] framework for these three Zn compounds.

In principle, the calculation of the optical properties can be considered the third step of the *ab initio* calculation starting with the determination of the ground state, followed by the application of the GW approach to obtain an accurate band structure, and finalized with the computation of the optical spectra.

The ground state is obtained from hybrid DFT with the HSE03 [27–29] functional as implemented in the Vienna Ab initio Simulation Package (VASP) [35]. We use experimental lattice constants, and the electron-ion interaction is described using the projector augmented-wave (PAW) method [36,37] with a plane-wave cutoff of 400 eV.

Based on the ground-state results, the QP energies are evaluated with a perturbative solution (G_0W_0) of the QP equation with the self-energy in the GW approximation [38]. We use the implementation according to Refs. [39–41]. Klimeš *et al.* [42] showed that quasiparticle GW calculations require careful convergence tests concerning the number of states in the calculation of the self-energy and the plane-wave cutoff in the response function to determine the screened Coulomb potential W. Additionally, the calculation of the optical properties requires a high **k**-point sampling. We use 160 states and a plane-wave cutoff of 200 eV for the response function together with a Γ-centered **k**-point sampling of up to $18 \times 18 \times 18$. The applied numerical parameters in the G_0W_0 calculations induce error bars for band energies of about 0.2 eV, as shown in Ref. [43]. The QP band gaps using these parameters, summarized in Table I, are close to the experimental values and, consequently, provide an accurate basis for the calculation of the nonlinear spectra. However, we also find that the calculated Zn $3d$ binding energies clearly deviate from measured values. This can, in some part, be improved by using GW PAW data sets or solving the QP equation self-consistently [41,58]. Focusing here on the optical properties, we refer to Ref. [43] for a detailed discussion of the band gaps and additionally the positions of the d states for the cubic Zn compounds. The influence of Zn $3d$ states on the nonlinear optical properties will be discussed below.

TABLE I. Lattice constants (in Å), band gaps E_g (in eV), high-frequency dielectric constants ϵ_∞, and Zn $3d$ binding energies (in eV) within hybrid DFT (HSE) and G_0W_0 for ZnS, ZnSe, and ZnTe used to compute the second-harmonic-generation spectra. The values are compared with experimental results from Refs. [44–57] (see Ref. [43] for details).

	ZnS	ZnSe	ZnTe
a	5.4102	5.6687	6.1035
E_g (HSE)	3.10	2.22	1.97
E_g (G_0W_0)	3.83	2.95	2.32
E_g (expt.)	3.66–3.84	2.7–2.83	2.18–2.39
ϵ_∞ (HSE)	5.15	5.97	7.37
ϵ_∞ (expt.)	5.13	5.4–6.3	7.1–7.4
Zn $3d$ (HSE)	7.43	7.84	8.42
Zn $3d$ (G_0W_0)	6.87	7.37	7.82
Zn $3d$ (expt.)	9.03	9.20, 8.9	9.84, 9.1

The exciton Hamiltonian is calculated following Refs. [11,59–61] for the linear optical properties to obtain the nonlinear optical response. In particular, the screening in the screened Coulomb potential W in Eq. (3) is described with the model dielectric function proposed by Bechstedt *et al.* [62] to reduce computation time. The high-frequency dielectric constants ϵ_∞ are required as input parameters for the model dielectric function. We use the HSE03 values calculated in Ref. [43], which are summarized in Table I and exhibit excellent agreement with experimental values [44,51–54,57].

To classify and discuss tendencies between different levels of theory for the SHG spectrum, we also calculate the dielectric function within the independent particle, the independent quasiparticle (IQA) approximations, and the BSE approach. In general, the hybrid-DFT energies $\epsilon_{n\mathbf{k}}$, which are used in IPA, are replaced by the corresponding G_0W_0 energies $\epsilon^{\mathrm{QP}}_{n\mathbf{k}}$ for the IQA. The optical matrix elements [see, e.g., Eq. (4) of Ref. [63]] entering the calculation of the dielectric function are evaluated according to the work of Gajdoš *et al.*[64] within the longitudinal approach. The momentum matrix elements, required for the calculation of the SHG spectrum, are obtained from the longitudinal approach [65],

$$p^\alpha_{mn}(\mathbf{k}) = \frac{m_e(\epsilon_{m\mathbf{k}} - \epsilon_{n\mathbf{k}})}{\hbar} \lim_{q\to 0} \frac{1}{q} \langle m\mathbf{k}|e^{iq\hat{r}_\alpha}|n\mathbf{k}\rangle \quad (23)$$

(with the position operator $\hat{r}_\alpha$), and rescaled according to

$$p^{\alpha,\mathrm{QP}}_{mn}(\mathbf{k}) = \frac{\epsilon^{\mathrm{QP}}_{m\mathbf{k}} - \epsilon^{\mathrm{QP}}_{n\mathbf{k}}}{\epsilon_{m\mathbf{k}} - \epsilon_{n\mathbf{k}}} p^\alpha_{mn}(\mathbf{k}) \quad (24)$$

in the IQA calculations, as proposed in Ref. [21]. This rescaling can be considered the introduction of an effective momentum operator accounting for nonlocal effects in the (QP) Hamiltonian [66]. The independent quasiparticle energies and momentum matrix elements also enter the computations corresponding to the BSE approach. We mention the study of Cabellos *et al.* [67], which shows that gauge invariance for SHG in the velocity gauge scheme (as used here) on the IQA level is not ensured with the rescaling of $p^\alpha_{mn}(\mathbf{k})$ according to Eq. (24). Instead, additional terms, which affect corrections in intensity and line shape of the SHG spectrum, are required

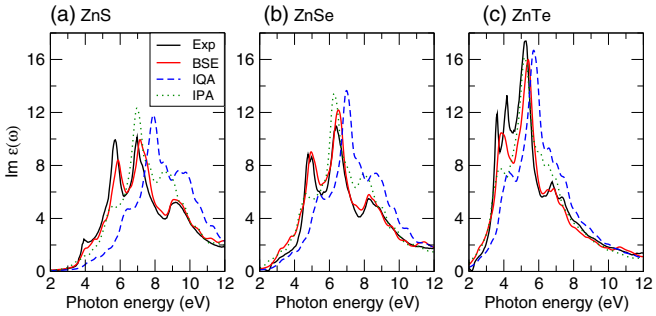

FIG. 1. Imaginary part of the dielectric function for (a) ZnS, (b) ZnSe, and (c) ZnSe calculated within the independent (quasi)particle approximation [IPA (IQA)] and within the Bethe-Salpeter approach (BSE). A Lorentzian broadening of $\eta = 0.2$ eV has been applied. The calculations are compared with measurements from Refs. [44,69] (Exp).

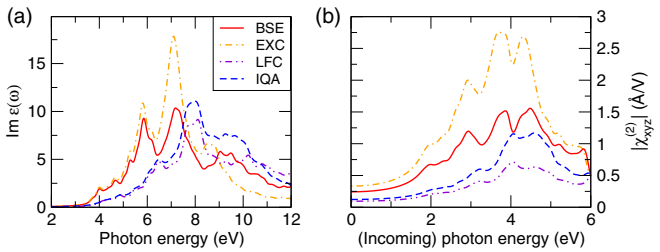

FIG. 2. Separate influence of local-field corrections (LFC) and excitonic effects (EXC) on (a) the dielectric function and (b) the SHG spectrum for ZnS compared with spectra computed within the independent quasiparticle approximation (IQA) and within the BSE approach (BSE). A Lorentzian broadening of $\eta = 0.15$ eV has been applied. The highest three valence and lowest five conduction bands have been included in the computations (see text for details).

to obtain gauge invariance for $\chi^{(2)}$. The inclusion of such corrections is, however, beyond the scope of the present study.

The calculation of the dielectric function is performed utilizing the time-evolution method [61,68]. Circumventing a diagonalization of the exciton Hamiltonian, a sufficient number of transitions between valence and conduction states can be included in the latter computation (e.g., Zn $3d$ states are also contained in the computation). However, a diagonalization of the excitonic matrix is required to evaluate the SHG spectra. To reduce the computational effort, the most strongly contributing valence and conduction states have been identified, and the effects related to the reduction of the number of $\mathbf{k}$ points are discussed in the following section.

IV. RESULTS

The computed optical absorption spectra for ZnS, ZnSe, and ZnTe are compared with measurements [44,69] at room temperature in Fig. 1. The comparison of the calculated results within the three levels of theory (IPA, IQA, and BSE) exposes the following tendencies: (i) One observes a blueshift of spectral features going from IPA to IQA, which is caused by the increased single-particle excitation energies within the G_0W_0 approach compared with hybrid DFT. (ii) The inclusion of excitonic and local-field effects causes a redistribution of oscillator strengths so that features in the dielectric function are redshifted and modified compared with IQA.

The separate impacts of local-field effects and the attractive electron-hole interaction on the dielectric function are also shown in Fig. 2(a). To account for local-field effects (or the electron-hole interaction) separately the spectrum has been calculated based on the excitonic matrix H^{ex}, discarding the third (second) line in Eq. (3) [i.e., with $W = 0$ ($\overline{v} = 0$)]. The comparison in Fig. 2(a) shows that local-field effects cause an overall reduction of the intensity, while the line shape is marginally affected. Similar observations have been made by Grüning and Attaccalite [20] for the cubic Zn compounds when comparing the particular independent particle spectrum (which is based on a band-gap-corrected band structure) and the spectrum computed within the random-phase approximation (RPA), which accounts for the inclusion of local-field corrections. The attractive electron-hole interaction, on the other hand, is responsible for the redshift of spectral features and for the oscillator-strength redistribution. The full BSE spectrum originates from the interplay of local-field and excitonic effects.

Although the BSE spectra generally show very good agreement with the measurements from Refs. [44,69], the following is to consider comparing the computed spectra with experimental data: Spin-orbit (SO) interaction is neglected in the present calculations. In particular ZnSe and ZnTe exhibit a strong SO split for the upper valence bands of ∼0.4 and ∼0.9 eV (see Refs. [70,71] and references therein). This causes a split of the respective first absorption peak in the absorption spectra of ZnSe and ZnTe [20,72,73].

Before a similar analysis of the influence of many-body effects can be performed for the nonlinear optical spectra, some additional notes on the numerical parameters are required. In particular, it is necessary to reduce the dimension of the excitonic matrix, which has to be diagonalized. One finds that Zn $3d$ states cause an average reduction of the SHG intensity by 11%, 9%, and 6% for ZnS, ZnSe, and ZnTe, respectively, on the level of IPA. The line shape is only marginally affected. Excluding Zn $3d$ states, computations of the SHG spectra with 512 $\mathbf{k}$ points show that it is sufficient to use the highest three valence and lowest five conduction states in the BSE calculations. In addition, we reduce the number of $\mathbf{k}$ points to $16 \times 16 \times 16$. Altogether, one finds that the main features remain conserved in the dielectric functions within the BSE approach and in the SHG spectra on the IPA level with these downscaled parameters. Therefore, excitonic matrices with a dimension of 61 440 have been diagonalized to compute the SHG tensors within the BSE approach.

The results for the SHG spectra are shown in Fig. 3. The present results are compared with measurements by Wagner *et al.* [24] and with recent calculations within the real-time TD-DPFT framework by Grüning and Attaccalite [20]. The spectra with the parameter-free approximations for the TDDFT exchange-correlation kernel, the jellium-with-gap model [74] (JGM), and the model proposed by Berger [75] to describe the polarization functional and within the real-time TDDFT with the Perdew-Burke-Ernzerhof (PBE) functional [76] (TD-PBE) from Ref. [20] are shown in Figs. 3 and 4.

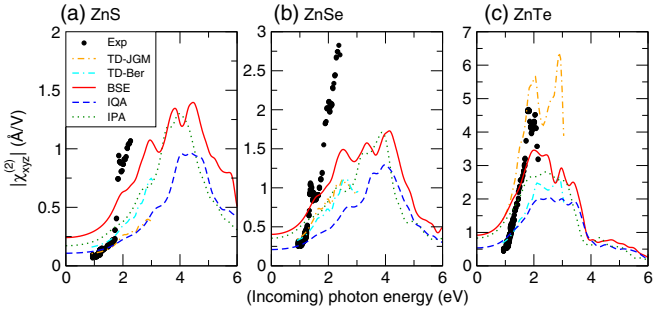

FIG. 3. SHG spectrum for (a) ZnS, (b) ZnSe, and (c) ZnTe calculated within the independent (quasi)particle approximation [IPA (IQA)] and within the Bethe-Salpeter approach (BSE). The BSE calculations have been performed without Zn 3*d* states (see text for further details). A Lorentzian broadening of $\eta = 0.2$ eV has been applied. The calculations are compared with measurements by Wagner *et al.* [24] (Exp) and calculations by Grüning and Attaccalite [20] within the real-time TD-DPFT framework approximating the polarization functional with the jellium-with-gap model [74] (TD-JGM) or with the model proposed by Berger [75] (TD-Ber).

Tendencies similar to those for the dielectric function are observed when comparing the three levels of theory (see Fig. 3). In particular, the blueshift of spectral features going from IPA to IQA is additionally accompanied by an intensity reduction. This is a consequence of the product of four excitation energy differences in the denominators of the SHG terms together with the rescaling of the momentum matrix elements [see also expression (B3)]. The intensity is essentially increased when taking excitonic and local-field effects into account. Up to some point, the peak structures in IPA can be recovered in the BSE spectra, but generally with different intensities. The separate impacts of local-field corrections and excitonic effects on the SHG spectrum can be seen from Fig. 2(b): Local-field effects mainly cause a uniform intensity reduction, while the electron-hole interaction redshifts spectral features, modifies the line shape, and increases the intensity.

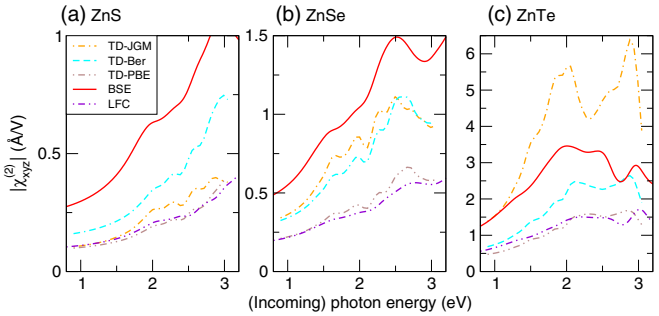

FIG. 4. SHG spectrum for (a) ZnS, (b) ZnSe, and (c) ZnSe accounting for local-field corrections (LFC) and calculated within the Bethe-Salpeter approach (BSE). The calculations have been performed without Zn 3*d* states (see text for further details). A Lorentzian broadening of $\eta = 0.2$ eV has been applied. The calculations are compared with those by Grüning and Attaccalite [20] within the real-time TD-DPFT framework approximating the polarization functional with the jellium-with-gap model [74] (TD-JGM) or with the model proposed by Berger [75] (TD-Ber) and with real-time TDDFT calculations with the PBE functional [76] (TD-PBE).

Similar observations about the influence of these two effects also have been made by Luppi *et al.* [14] while studying the SHG spectra of SiC, AlAs, and GaAs within the TDDFT framework utilizing the static long-range kernel [77].

The basis for the comparison of the present results with the calculations performed by Grüning and Attaccalite is given by the fact that in both cases a similar band structure has been applied (i.e., a PBE band structure with a corrected band gap to reproduce the experimental value in Ref. [20] and the HSE+G_0W_0 band structure in the present study). The comparison of the relevant spectra is given in Fig. 4. The coincidence between the TD-PBE spectra and the SHG spectra accounting for local-field corrections is clearly visible from Fig. 4. This can be explained by the experience [20] that standard TDDFT spectra are close to those obtained within the RPA accounting for local-field corrections within the TDDFT. The additional inclusion of the excitonic contribution, either within the real-time TD-DPFT framework or within the BSE approach, particularly results in an intensity increase. The intensity of the BSE spectra is by a factor of 3 to 1.3 larger than the intensity of the corresponding spectra within the real-time TD-DPFT framework for ZnS, ZnSe, and ZnTe (with the model proposed by Berger [75]). The exception is the SHG spectrum of ZnTe within the real-time TD-DPFT framework employing the JGM [74], which generally exceeds the intensity of the BSE spectrum. Therefore, the present approach mostly suggests stronger excitonic effects than observed within the real-time TD-DPFT framework in Ref. [20].

Comparing the BSE spectra with measurements by Wagner *et al.*, one finds that the present BSE calculations overestimate the experimental intensities by factors of 2 to 3 in the low-frequency region (i.e., at $\hbar\omega \simeq 1$ eV). The measured intensity is underestimated by a factor of 2 for ZnS and ZnSe as well as by factor of 1.6 for ZnTe for energies about 2 eV. Although the BSE spectra tend to come closer to the experimental results than the IPA/IQA spectra for ZnS and ZnTe, the visible deviations for SHG are clearly in contrast to the agreement between the BSE spectra with the measurements for the dielectric function. It has also been checked that estimated horizontal error bars, given by 20% of the intensity for the measurements [24] (see also Fig. 10 in Ref. [20]) and estimated by 15% intensity reduction for the calculations (due to the exclusion of Zn 3*d* states), and vertical error bars, estimated by the accuracy of the band structure calculation (∼0.2 eV) and temperature effects [46,78,79] (∼0.1 eV), do not change the above conclusion at that point. Finally, the influence of the SO interaction and gauge-invariance-related corrections [67] on the SHG spectrum may also contribute to the deviations between experiment and theory.

V. CONCLUSIONS

We used the theory of Leitsmann *et al.* [21], which accounts for excitonic and local-field effects in the linear and nonlinear optical responses, to study the second-harmonic-generation spectrum of ZnS, ZnSe, and ZnTe from first principles. We showed how this methodology can be extended to the limit $\omega \to 0$. A major drawback of the present method is that the excitonic matrix has to be diagonalized to obtain the SHG spectrum. A similar influence of excitonic and local-field

effects, i.e., a redshift of features in the spectrum with additional line-shape modification compared with independent particle calculations, is observed for the dielectric function and for the second-harmonic-generation spectrum. More precisely, local-field effects mainly decrease the intensity, while excitonic effects increase the intensity, modify the line shape, and redshift spectral features. The computed results for the nonlinear optical spectrum have been compared with time-dependent density (-polarization) functional theory calculations in the real-time framework by Grüning and Attaccalite [20] as well as with measurements by Wagner *et al.* [24]. The SHG spectra obtained within the real-time TDDFT with the PBE functional, which are close to spectra computed within the RPA, agree with the present calculations accounting for local-field corrections. In most cases, the calculations within the present approach suggest larger excitonic effects than obtained within the real-time TD-DPFT [20] framework. The comparison with measurements [24] showed that, although the BSE spectra for ZnS and ZnTe are closer to the experiment than the spectra within the IPA and IQA, clear deviations are still apparent.

ACKNOWLEDGMENTS

The Deutsche Forschungsgemeinschaft (DFG) is acknowledged for financial support via the SFB/TRR 142, project B04. The calculations were performed at the Paderborn Center for Parallel Computing (PC^2) and at the High Performance Computing Center in Stuttgart (HLRS).

APPENDIX A: DIVERGENT SHG CONTRIBUTIONS

The functions A_i and B_i in Eqs. (11) and (12) are given by (with $\tilde{\epsilon} := \hbar\tilde{\omega}$)

$$A_1(\tilde{\epsilon}, E_\Lambda, E_{\Lambda'}) = \frac{1}{(2\,E_\Lambda - E_{\Lambda'})(E_\Lambda + \tilde{\epsilon})E_\Lambda^3}, \tag{A1}$$

$$A_2(\tilde{\epsilon}, E_\Lambda, E_{\Lambda'}) = -\frac{16}{(2\,E_\Lambda - E_{\Lambda'})(E_{\Lambda'} + 2\,\tilde{\epsilon})E_{\Lambda'}^3}, \tag{A2}$$

$$A_3(\tilde{\epsilon}, E_\Lambda, E_{\Lambda'}) = \frac{1}{E_\Lambda E_{\Lambda'}\tilde{\epsilon}^3}, \tag{A3}$$

$$A_4(\tilde{\epsilon}, E_\Lambda, E_{\Lambda'}) = -\frac{2\,E_\Lambda + E_{\Lambda'}}{E_\Lambda^2 E_{\Lambda'}^2\tilde{\epsilon}^2}, \tag{A4}$$

$$A_5(\tilde{\epsilon}, E_\Lambda, E_{\Lambda'}) = \frac{4\,E_\Lambda^2 + 2\,E_\Lambda E_{\Lambda'} + E_{\Lambda'}^2}{E_\Lambda^3 E_{\Lambda'}^3\tilde{\epsilon}} \tag{A5}$$

and

$$B_1(\tilde{\epsilon}, E_\Lambda, E_{\Lambda'}) = \frac{1}{(E_\Lambda + E_{\Lambda'})(E_\Lambda + \tilde{\epsilon})E_\Lambda^3}, \tag{A6}$$

$$B_2(\tilde{\epsilon}, E_\Lambda, E_{\Lambda'}) = -\frac{16}{(E_\Lambda + E_{\Lambda'})(E_\Lambda - E_{\Lambda'} + 2\,\tilde{\epsilon})(E_\Lambda - E_{\Lambda'})^3}, \tag{A7}$$

$$B_3(\tilde{\epsilon}, E_\Lambda, E_{\Lambda'}) = \frac{1}{(E_\Lambda - E_{\Lambda'})E_\Lambda\tilde{\epsilon}^3}, \tag{A8}$$

$$B_4(\tilde{\epsilon}, E_\Lambda, E_{\Lambda'}) = -\frac{3\,E_\Lambda - E_{\Lambda'}}{(E_\Lambda - E_{\Lambda'})^2 E_\Lambda^2\tilde{\epsilon}^2}, \tag{A9}$$

$$B_5(\tilde{\epsilon}, E_\Lambda, E_{\Lambda'}) = \frac{7\,E_\Lambda^2 - 4\,E_\Lambda E_{\Lambda'} + E_{\Lambda'}^2}{(E_\Lambda - E_{\Lambda'})^3 E_\Lambda^3\tilde{\epsilon}}. \tag{A10}$$

It will be shown in the following that the contributions to the SHG tensor arising from A_3–A_5 and B_2–B_5 vanish.

Exploiting the property

$$B_2(\tilde{\epsilon}, E_\Lambda, E_{\Lambda'}) = B_2(-\tilde{\epsilon}, E_{\Lambda'}, E_\Lambda) \tag{A11}$$

together with Eq. (10), it is straightforward to show that this contribution vanishes. The cancellation of contributions related to A_3–A_5 and B_3–B_5 can be shown by taking time–reversal symmetry into account. Time-reversal symmetry implies that

$$\psi_{n\mathbf{k}}(\mathbf{r}) = [\psi_{n\bar{\mathbf{k}}}(\mathbf{r})]^*, \quad p_{ij}(\mathbf{k}) = -[p_{ij}(\bar{\mathbf{k}})]^*, \quad \epsilon_{n\mathbf{k}} = \epsilon_{n\bar{\mathbf{k}}}, \tag{A12}$$

with $\bar{\mathbf{k}} := -\mathbf{k}$ for simplicity. One can directly show for the exciton Hamiltonian (3) with Eqs. (A12) that

$$H^{\mathrm{ex}}_{vc\mathbf{k},v'c'\mathbf{k}'} = \left[H^{\mathrm{ex}}_{vc\bar{\mathbf{k}},v'c'\bar{\mathbf{k}}'}\right]^*. \tag{A13}$$

At this point, one way to proceed is to apply the spectral theorem for Hermitian matrices. One can show by induction for real functions $f(E_\Lambda), f'(E_\Lambda) \propto E_\Lambda^{\pm n}$ (with $n > 0$ being integer and the *one-to-one* correspondence between $\mathbf{k}$ and $\bar{\mathbf{k}}$ in the BZ required)

$$\begin{aligned}[f(H^{\mathrm{ex}})]_{vc\mathbf{k},v'c'\mathbf{k}'} &= \sum_\Lambda f(E_\Lambda) A_\Lambda^{cv}(\mathbf{k})\left[A_\Lambda^{c'v'}(\mathbf{k}')\right]^* \\ &= \sum_\Lambda f(E_\Lambda)\left[A_\Lambda^{cv}(\bar{\mathbf{k}})\right]^* A_\Lambda^{c'v'}(\bar{\mathbf{k}}'). \end{aligned} \tag{A14}$$

It follows for the auxiliary functions Π and Z that

$$\sum_\Lambda f(E_\Lambda)\Pi_\alpha(\Lambda, cv\mathbf{k}) = (-1)\sum_\Lambda f(E_\Lambda)\left[\Pi_\alpha(\Lambda, cv\bar{\mathbf{k}})\right]^* \tag{A15}$$

and

$$\begin{aligned}&\sum_{\Lambda\Lambda'} f(E_\Lambda) f'(E_{\Lambda'}) Z_{\alpha\beta\gamma}(\Lambda, \Lambda', cv\mathbf{k}) \\ &\quad = (-1)\sum_{\Lambda\Lambda'} f(E_\Lambda) f'(E_{\Lambda'})[Z_{\alpha\beta\gamma}(\Lambda, \Lambda', cv\bar{\mathbf{k}})]^*. \end{aligned} \tag{A16}$$

Considering the A_3 contribution, one has to add up contributions similar to

$$\begin{aligned}&\sum_{\Lambda\Lambda'}\sum_{cv\mathbf{k}}\{A_3(\tilde{\epsilon}, \Lambda, \Lambda')\,[Z_{\alpha\gamma\beta}(\Lambda', \Lambda, cv\mathbf{k})]^* \\ &\qquad - A_3(-\tilde{\epsilon}, \Lambda, \Lambda')\,Z_{\alpha\gamma\beta}(\Lambda', \Lambda, cv\mathbf{k})\} \\ &\quad = \frac{1}{\tilde{\epsilon}^3}\sum_{\Lambda\Lambda'}\sum_{cv\mathbf{k}}\frac{1}{E_\Lambda E_{\Lambda'}}\{[Z_{\alpha\gamma\beta}(\Lambda', \Lambda, cv\mathbf{k})]^* \\ &\qquad + Z_{\alpha\gamma\beta}(\Lambda', \Lambda, cv\mathbf{k})\}, \end{aligned}$$

which vanish due to time-reversal symmetry (A16) and since one has for integration of a function $g(\mathbf{k})$ over the whole BZ

$$\int_{\mathrm{BZ}} d^3k\, g(\mathbf{k}) = \int_{\mathrm{BZ}} d^3k\, g(\bar{\mathbf{k}}). \tag{A17}$$

Another way to utilize the time-reversal symmetry of the excitonic matrix (A13) is described in Appendix C and results from the fact that only Im(Z) contributes to the SHG spectrum.

Taking additionally the algebraic property of Z [Eq. (10)] into account, it can be shown with the same procedure that the contributions related to A_5, B_3, and B_5 vanish independently of each other. The cancellation of contributions related to A_4 together with B_4 can be shown for crystals exhibiting the zinc-blende structure utilizing

$$\chi^{(2)}_{\alpha\beta\gamma} = \tfrac{1}{3}\big[\chi^{(2)}_{\alpha\beta\gamma} + \chi^{(2)}_{\beta\gamma\alpha} + \chi^{(2)}_{\gamma\alpha\beta}\big] \tag{A18}$$

and

$$A_4(\tilde{\epsilon}, E_\Lambda, E_{\Lambda'}) - A_4(\tilde{\epsilon}, E_{\Lambda'}, E_\Lambda) = B_4(\tilde{\epsilon}, E_\Lambda, E_{\Lambda'}) - B_4(\tilde{\epsilon}, E_{\Lambda'}, E_\Lambda) = \frac{E_{\Lambda'} - E_\Lambda}{E_\Lambda^2 E_{\Lambda'}^2 \tilde{\epsilon}^2}. \tag{A19}$$

APPENDIX B: CROSSOVER BETWEEN BSE AND IPA APPROACH

The three-band contribution of the IPA SHG equations are given in Eq. (32) of Ref. [21] by (with $\hbar\omega_{mn}(\mathbf{k}) := \epsilon_{m\mathbf{k}} - \epsilon_{n\mathbf{k}}$)

$$\chi^{(2),\mathrm{three}}_{\alpha\beta\gamma}(-2\omega,\omega,\omega) = -\frac{ie^3}{m_e^3\hbar^2 V}\sum_{n,m,l}{}' \sum_{\mathbf{k}} \frac{p^\alpha_{nm}(\mathbf{k})\{p^\beta_{ml}(\mathbf{k})p^\gamma_{ln}(\mathbf{k})\}_+}{\omega_{ln}(\mathbf{k}) - \omega_{ml}(\mathbf{k})}\left(\frac{16 f_{nm}(\mathbf{k})}{[\omega_{mn}(\mathbf{k})]^3[\omega_{mn}(\mathbf{k}) - 2\tilde{\omega}]}\right.$$
$$\left. + \frac{f_{ml}(\mathbf{k})}{[\omega_{ml}(\mathbf{k})]^3[\omega_{ml}(\mathbf{k}) - \tilde{\omega}]} + \frac{f_{ln}(\mathbf{k})}{[\omega_{ln}(\mathbf{k})]^3[\omega_{ln}(\mathbf{k}) - \tilde{\omega}]}\right). \tag{B1}$$

The prime in the sum denotes that the summation runs over all single-particle states with $n \neq m \neq l$. We use the abbreviation

$$\big\{p^\beta_{ml}(\mathbf{k})p^\gamma_{ln}(\mathbf{k})\big\}_+ = \tfrac{1}{2}\big[p^\beta_{ml}(\mathbf{k})p^\gamma_{ln}(\mathbf{k}) + p^\gamma_{ml}(\mathbf{k})p^\beta_{ln}(\mathbf{k})\big]. \tag{B2}$$

Applying the occupation number differences $f_{nm} = 0, -1, 1$ in the second addend of Eq. (B1), one finds

$$-\frac{ie^3}{m_e^3\hbar^2 V}\sum_{\mathbf{k}}\left\{\sum_{vv'c}{}' \frac{p^\alpha_{vv'}(\mathbf{k})\big\{p^\beta_{v'c}(\mathbf{k})p^\gamma_{cv}(\mathbf{k})\big\}_+}{\omega_{cv}(\mathbf{k}) + \omega_{cv'}(\mathbf{k})}\frac{1}{\omega_{cv'}(\mathbf{k})^3[\omega_{cv'}(\mathbf{k}) + \tilde{\omega}]} + \sum_{vv'c}{}' \frac{p^\alpha_{vc}(\mathbf{k})\big\{p^\beta_{cv'}(\mathbf{k})p^\gamma_{v'v}(\mathbf{k})\big\}_+}{2\omega_{cv'}(\mathbf{k}) - \omega_{cv}(\mathbf{k})}\frac{1}{\omega_{cv'}(\mathbf{k})^3[\omega_{cv'}(\mathbf{k}) - \tilde{\omega}]}\right.$$
$$\left. + \sum_{cc'v}{}' \frac{p^\alpha_{cv}(\mathbf{k})\big\{p^\beta_{vc'}(\mathbf{k})p^\gamma_{c'c}(\mathbf{k})\big\}_+}{2\omega_{c'v}(\mathbf{k}) - \omega_{cv}(\mathbf{k})}\frac{1}{\omega_{c'v}(\mathbf{k})^3[\omega_{c'v}(\mathbf{k}) + \tilde{\omega}]} + \sum_{cc'v}{}' \frac{p^\alpha_{cc'}(\mathbf{k})\big\{p^\beta_{c'v}(\mathbf{k})p^\gamma_{vc}(\mathbf{k})\big\}_+}{\omega_{cv}(\mathbf{k}) + \omega_{c'v}(\mathbf{k})}\frac{1}{\omega_{c'v}(\mathbf{k})^3[\omega_{c'v}(\mathbf{k}) - \tilde{\omega}]}\right\} \tag{B3}$$

On the other hand, using the IPA expressions (14) and (15), one finds for Z [see Eq. (5)]

$$\text{IPA:}\quad Z_{\alpha\beta\gamma}(\Lambda,\Lambda',cv\mathbf{k}) = \sum_{c'}\big[p^\alpha_{cv}(\mathbf{k})\big]^*\,\delta_{\Lambda,cv\mathbf{k}}\,p^\beta_{c'v}(\mathbf{k})\delta_{\Lambda',c'v\mathbf{k}}\,p^\gamma_{cc'}(\mathbf{k}) - \sum_{v'}\big[p^\alpha_{cv}(\mathbf{k})\big]^*\,\delta_{\Lambda,cv\mathbf{k}}\,p^\beta_{cv'}(\mathbf{k})\delta_{\Lambda',cv'\mathbf{k}}\,p^\gamma_{v'v}(\mathbf{k}). \tag{B4}$$

Note that the triple $(cv\mathbf{k})$ is mapped on a single integer index. Employing the IPA expressions of the matrices Z in the BSE-related equation (13), one finds that the IPA and BSE contributions with the prefactor 16 are related. Additionally, it can be concluded from expression (B3) that the second (and analogously the third) IPA addend [in Eq. (B1)] contains contributions related to the remaining $(2E_\Lambda - E_{\Lambda'})^{-1}$ terms as well as to the $(E_\Lambda + E_{\Lambda'})^{-1}$ terms in Eq. (13).

APPENDIX C: SIMPLIFICATION WITH TIME-REVERSAL SYMMETRY

It can be found with Eqs. (A13) and (A17) that

$$\sum_{c'v'\mathbf{k}'} H_{vc\mathbf{k},v'c'\mathbf{k}'}\big[A^{c'v'}_\Lambda(\bar{\mathbf{k}}')\big]^* = E_\Lambda\big[A^{cv}_\Lambda(\bar{\mathbf{k}})\big]^*. \tag{C1}$$

This reveals that $B^{cv}_\Lambda(\mathbf{k}) := [A^{cv}_\Lambda(\bar{\mathbf{k}})]^*$ (note the one-to-one correspondence between $\mathbf{k}$ and $\bar{\mathbf{k}}$ in the BZ) are also excitonic eigenvectors to the eigenenergies E_Λ. Consequently, the basic SHG equation (7) can be rewritten with B_Λ instead of A_Λ. One can define appropriate auxiliary functions $\tilde{\Pi}$ and $\tilde{Z}$ with the properties

$$\tilde{\Pi}_\alpha(\Lambda,cv\mathbf{k}) := B^{cv}_\Lambda(\mathbf{k})\sum_{c'v'\mathbf{k}'} p^\alpha_{c'v'}(\mathbf{k}')\big[B^{c'v'}_\Lambda(\mathbf{k}')\big]^* \tag{C2}$$
$$= -[\Pi_\alpha(\Lambda,cv\bar{\mathbf{k}})]^* \tag{C3}$$

and

$$\tilde{Z}_{\alpha\beta\gamma}(\Lambda,\Lambda') = -[Z_{\alpha\beta\gamma}(\Lambda,\Lambda')]^*. \tag{C4}$$

The consequence is that only Im(Z) contributes to the SHG spectrum.

[1] S. Albrecht, L. Reining, R. D. Sole, and G. Onida, Phys. Rev. Lett. **80**, 4510 (1998).

[2] L. X. Benedict, E. L. Shirley, and R. B. Bohn, Phys. Rev. B **57**, R9385 (1998).

[3] M. Rohlfing and S. G. Louie, Phys. Rev. Lett. **81**, 2312 (1998).

[4] G. Onida, L. Reining, and A. Rubio, Rev. Mod. Phys. **74**, 601 (2002).

[5] L. Hedin and S. O. Lundqvist, in *Solid State Physics*, edited by F. Seitz, D. Turnbull, and H. Ehrenreich (Academic Press, New York, 1969), Vol. 23, pp. 1–181.
[6] F. Aryasetiawan and O. Gunnarsson, Rep. Prog. Phys. **61**, 237 (1998).
[7] L. Hedin, Phys. Rev. **139**, A796 (1965).
[8] L. J. Sham and T. M. Rice, Phys. Rev. **144**, 708 (1966).
[9] W. Hanke and L. J. Sham, Phys. Rev. Lett. **43**, 387 (1979).
[10] G. Strinati, Riv. Nuovo Cimento **11**, 1 (1988).
[11] P. H. Hahn, W. G. Schmidt, and F. Bechstedt, Phys. Rev. Lett. **88**, 016402 (2001).
[12] Y. R. Shen, Solid State Commun. **102**, 221 (1997).
[13] J. F. McGilp, J. Phys. D **29**, 1812 (1996).
[14] E. Luppi, H. Hübener, and V. Véniard, Phys. Rev. B **82**, 235201 (2010).
[15] C. Attaccalite and M. Grüning, Phys. Rev. B **88**, 235113 (2013).
[16] C. Attaccalite, M. Grüning, and A. Marini, Phys. Rev. B **84**, 245110 (2011).
[17] M. Grüning and C. Attaccalite, Phys. Rev. B **89**, 081102 (2014).
[18] M. Grüning and C. Attaccalite, Phys. Rev. B **90**, 199901(E) (2014).
[19] C. Attaccalite, A. Nguer, E. Cannuccia, and M. Gruning, Phys. Chem. Chem. Phys. **17**, 9533 (2015).
[20] M. Grüning and C. Attaccalite, Phys. Chem. Chem. Phys. **18**, 21179 (2016).
[21] R. Leitsmann, W. G. Schmidt, P. H. Hahn, and F. Bechstedt, Phys. Rev. B **71**, 195209 (2005).
[22] E. K. Chang, E. L. Shirley, and Z. H. Levine, Phys. Rev. B **65**, 035205 (2001).
[23] M. L. Trolle, G. Seifert, and T. G. Pedersen, Phys. Rev. B **89**, 235410 (2014).
[24] H. P. Wagner, M. Kühnelt, W. Langbein, and J. M. Hvam, Phys. Rev. B **58**, 10494 (1998).
[25] T. G. Pedersen and H. D. Cornean, Europhys. Lett. **78**, 27005 (2007).
[26] P. N. Butcher and D. Cotter, *The Elements of Nonlinear Optics* (Cambridge University Press, Cambridge, 1990).
[27] J. Heyd, G. E. Scuseria, and M. Ernzerhof, J. Chem. Phys. **118**, 8207 (2003).
[28] J. Heyd and G. E. Scuseria, J. Chem. Phys. **121**, 1187 (2004).
[29] A. V. Krukau, O. A. Vydrov, A. F. Izmaylov, and G. E. Scuseria, J. Chem. Phys. **125**, 224106 (2006).
[30] W. G. Aulbur, L. Jönsson, and J. W. Wilkins, in *Solid State Physics*, edited by H. Ehrenreich and F. Spaepen (Academic Press, San Diego, 2000), Vol. 54, pp. 1–218.
[31] F. Bechstedt, F. Fuchs, and G. Kresse, Phys. Status Solidi B **246**, 1877 (2009).
[32] S. V. Faleev, M. van Schilfgaarde, and T. Kotani, Phys. Rev. Lett. **93**, 126406 (2004).
[33] E. Ghahramani, D. J. Moss, and J. E. Sipe, Phys. Rev. B **43**, 8990 (1991).
[34] D. E. Aspnes, Phys. Rev. B **6**, 4648 (1972).
[35] G. Kresse and J. Furthmüller, Comput. Mater. Sci. **6**, 15 (1996).
[36] P. E. Blöchl, Phys. Rev. B **50**, 17953 (1994).
[37] G. Kresse and D. Joubert, Phys. Rev. B **59**, 1758 (1999).
[38] M. S. Hybertsen and S. G. Louie, Phys. Rev. B **34**, 5390 (1986).
[39] M. Shishkin and G. Kresse, Phys. Rev. B **74**, 035101 (2006).
[40] M. Shishkin and G. Kresse, Phys. Rev. B **75**, 235102 (2007).
[41] M. Shishkin, M. Marsman, and G. Kresse, Phys. Rev. Lett. **99**, 246403 (2007).
[42] J. Klimeš, M. Kaltak, and G. Kresse, Phys. Rev. B **90**, 075125 (2014).
[43] A. Riefer, N. Weber, J. Mund, D. R. Yakovlev, M. Bayer, A. Schindlmayr, C. Meier, and W. G. Schmidt, J. Phys. Condens. Matter **29**, 215702 (2017).
[44] M. Cardona and G. Harbeke, Phys. Rev. **137**, A1467 (1965).
[45] D. Theis, Phys. Status Solidi B **79**, 125 (1977).
[46] R. Pässler, E. Griebl, H. Riepl, G. Lautner, S. Bauer, H. Preis, W. Gebhardt, B. Buda, D. J. As, D. Schikora, K. Lischka, K. Papagelis, and S. Ves, J. Appl. Phys. **86**, 4403 (1999).
[47] W. H. Strehlow and E. L. Cook, J. Phys. Chem. Ref. Data **2**, 163 (1973).
[48] S. Ves, K. Strössner, N. E. Christensen, C. K. Kim, and M. Cardona, Solid State Commun. **56**, 479 (1985).
[49] M. Aven, D. T. F. Marple, and B. Segall, J. Appl. Phys. **32**, 2261 (1961).
[50] R. E. Nahory and H. Y. Fan, Phys. Rev. **156**, 825 (1967).
[51] D. C. Reynolds, C. W. Litton, and T. C. Collins, Phys. Status Solidi B **12**, 3 (1965).
[52] S. J. Czyzak, W. M. Baker, R. C. Crane, and J. B. Howe, J. Opt. Soc. Am. **47**, 240 (1957).
[53] *II-VI and I-VII Compounds: Semimagnetic Compounds*, Vol. 41B, edited by O. Madelung, U. Rössler, and M. Schulz (Springer, Berlin, 1999), pp. 1–6.
[54] E. Constable and R. A. Lewis, J. Appl. Phys. **112**, 063104 (2012).
[55] L. Ley, R. A. Pollak, F. R. McFeely, S. P. Kowalczyk, and D. A. Shirley, Phys. Rev. B **9**, 600 (1974).
[56] C. J. Vesely, R. L. Hengehold, and D. W. Langer, Phys. Rev. B **5**, 2296 (1972).
[57] *II-VI and I-VII Compounds: Semimagnetic Compounds*, Vol. 41B, edited by O. Madelung, U. Rössler, and M. Schulz (Springer, Berlin, 1999), pp. 1–5.
[58] M. van Schilfgaarde, T. Kotani, and S. Faleev, Phys. Rev. Lett. **96**, 226402 (2006).
[59] C. Rödl, F. Fuchs, J. Furthmüller, and F. Bechstedt, Phys. Rev. B **77**, 184408 (2008).
[60] F. Fuchs, C. Rödl, A. Schleife, and F. Bechstedt, Phys. Rev. B **78**, 085103 (2008).
[61] W. G. Schmidt, S. Glutsch, P. H. Hahn, and F. Bechstedt, Phys. Rev. B **67**, 085307 (2003).
[62] F. Bechstedt, R. D. Sole, G. Cappellini, and L. Reining, Solid State Commun. **84**, 765 (1992).
[63] A. Riefer, F. Fuchs, C. Rödl, A. Schleife, F. Bechstedt, and R. Goldhahn, Phys. Rev. B **84**, 075218 (2011).
[64] M. Gajdoš, K. Hummer, G. Kresse, J. Furthmüller, and F. Bechstedt, Phys. Rev. B **73**, 045112 (2006).
[65] F. Bechstedt, *Many-Body Approach to Electronic Excitations: Concepts and Applications* (Springer, Heidelberg, 2015), Chap. 20.
[66] R. D. Sole and R. Girlanda, Phys. Rev. B **48**, 11789 (1993).
[67] J. L. Cabellos, B. S. Mendoza, M. A. Escobar, F. Nastos, and J. E. Sipe, Phys. Rev. B **80**, 155205 (2009).
[68] S. Glutsch, D. S. Chemla, and F. Bechstedt, Phys. Rev. B **54**, 11592 (1996).
[69] J. L. Freeouf, Phys. Rev. B **7**, 3810 (1973).
[70] P. Carrier and S.-H. Wei, Phys. Rev. B **70**, 035212 (2004).

[71] S. Zh. Karazhanov, P. Ravindran, A. Kjekshus, H. Fjellvěg, U. Grossner, and B. G. Svensson, J. Appl. Phys. **100**, 043709 (2006).
[72] J. P. Walter, M. L. Cohen, Y. Petroff, and M. Balkanski, Phys. Rev. B **1**, 2661 (1970).
[73] S. Zh. Karazhanov, P. Ravindran, A. Kjekshus, H. Fjellvåg, and B. G. Svensson, Phys. Rev. B **75**, 155104 (2007).
[74] P. E. Trevisanutto, A. Terentjevs, L. A. Constantin, V. Olevano, and F. D. Sala, Phys. Rev. B **87**, 205143 (2013).
[75] J. A. Berger, Phys. Rev. Lett. **115**, 137402 (2015).
[76] J. P. Perdew, K. Burke, and M. Ernzerhof, Phys. Rev. Lett. **77**, 3865 (1996).
[77] S. Botti, F. Sottile, N. Vast, V. Olevano, L. Reining, H.-C. Weissker, A. Rubio, G. Onida, R. D. Sole, and R. W. Godby, Phys. Rev. B **69**, 155112 (2004).
[78] Y. F. Tsay, S. S. Mitra, and J. F. Vetelino, J. Phys. Chem. Solids **34**, 2167 (1973).
[79] J. Camassel and D. Auvergne, Phys. Rev. B **12**, 3258 (1975).